

Hybrid Mach-Zehnder interferometric sensor based on two core-offset attenuators and an abrupt taper in single-mode fiber

Le Xu (徐 乐), Weina Han (韩伟娜), Peng Wang (王 鹏), and Sumei Wang (王素梅)*

Laser Micro/Nano-Fabrication Laboratory, School of Mechanical Engineering,
Beijing Institute of Technology, Beijing 100081, China

*Corresponding author: wangsumeibit@bit.edu.cn

Received February 12, 2014; accepted April 23, 2014; posted online June 25, 2014

This study proposes a new hybrid Mach-Zehnder interferometric (MZI) sensor based on two core-offset attenuators and an abrupt taper in a single-mode fiber fabricated by a fiber-taper machine and electric arc discharge. When the distance between the two core-offset attenuators is stretched to 4500 μm , significant interference signals are detected with a prominent attenuation peak of ~ 28 dB. The proposed MZI can be used to measure temperature due to its low refractive index (RI) and strain cross-sensitivity. The temperature sensitivity is 34.95 ± 0.04 and 106.70 ± 0.04 $\text{pm}/^\circ\text{C}$ in the temperature ranges of 14–250 and 250–1000 $^\circ\text{C}$, respectively.

OCIS codes: 060.2280, 060.2370.

doi: 10.3788/COL201412.070602.

Fiber sensors are widely applied to monitor physical, chemical, and biological parameters for process control in the manufacturing, biomedical, aerospace, petrochemical, and public health industries due to their unique advantages, such as compact size, low cost, and immunity to electromagnetic interference^[1]. The physical quantities, including refractive index (RI), stress, gas concentrations, and temperature, are important parameters in these applications^[2]. Among various fiber optic techniques, fiber-based interferometer sensors have special advantages, such as high sensitivity, high integration, simplicity, and compact inline measurement. The types of optical fiber sensors in a single-mode fiber (SMF) include the Fabry-Perot^[3], long-period gratings (LPGs)^[4,5], Mach-Zehnder^[6,7], and Michelson interferometers^[8,9]. Various methods were proposed to fabricate the sensors, including splicing two pieces of a photonic crystal fiber (PCF) with a small lateral offset^[10], two abrupt tapers^[11], a biconical fiber taper^[12], a single abrupt taper in a SMF with a cleaved-fiber, coated end^[13,14], an intrinsic Fabry-Perot interferometer fabricated at the fiber tip^[15,16], etc. A few sensors can measure RI and temperature simultaneously by using LPGs, modified fiber Bragg gratings (FBGs), and hybrid LPG-FBG structures^[17–19]. Yet they do possess some disadvantages, such as an unstable system and high cost, which restrict their industrial applications. Fabry-Perot fiber sensors and core diameter mismatch interferometers can measure temperatures up to ~ 1000 $^\circ\text{C}$, but these sensors all have cross-sensitivity to external RI^[20].

In this study, a sensor consisting of two core-offset attenuators and an abrupt taper is proposed and fabricated by a fiber-taper machine and electric arc discharge on SMF. The temperature sensitivity is 34.95 ± 0.04 and 106.70 ± 0.04 $\text{pm}/^\circ\text{C}$ in the temperature ranges of 14–250 and 250–1000 $^\circ\text{C}$, respectively. The cross-sensitivities of the proposed sensor to external RI and strain are low,

which is desirable for temperature sensing.

Figure 1 illustrates the schematic structure of the interferometer sensor. One offset attenuator is completed through fusion splicing of two sections of SMF; the other offset attenuator is fabricated in the same way. An abrupt fiber taper is then pulled between the two core-offset attenuators by a fiber-taper machine. Part of the incident lights are coupled into the tapered cladding from the core after they pass through the first offset attenuator, and then coupled back into the core when they pass through the second offset attenuator. The phase difference between the cladding and the core modes can be expressed as^[1]

$$\phi = \frac{2\pi\Delta n_{\text{eff}}L}{\lambda_m}, \quad (1)$$

where Δn_{eff} is the difference of the effective RI between the core and the cladding modes, L is the length of the interferometer, and λ_m is the wavelength of the attenuation peak in air. When the phase difference is an integral number of π , i.e. $\phi = (2m + 1)\pi$, the wavelength of the attenuation peaks is approximated by^[21]

$$\lambda_m = \frac{2\Delta n_{\text{eff}}L}{2m + 1}. \quad (2)$$

When the difference of the effective RI (Δn_{eff}) has a small incremental δn_{eff} with the external indexes, the wavelength of the attenuation peak shifts to a shorter distance with the change of the external indexes. According

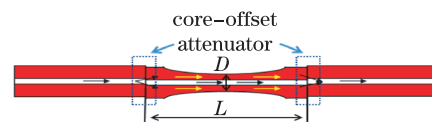


Fig. 1. Schematic structure of the interferometer based on two offset attenuators and an abrupt taper.

to Eqs. (1) and (2), the distance can be expressed by

$$\delta\lambda_m = \frac{2L\delta n_{\text{eff}}}{2m+1}, \quad (3)$$

where $\delta\lambda_m/\delta n_{\text{eff}}$ expresses the sensitivity of this sensor. The change of external index (e.g. the length of sensor or the effective RI) can induce wavelength shift $\delta\lambda_m$. Through Eq. (3), the sensitivity of the sensor can be improved by increasing the length L or decreasing the fringe order m .

The fiber in-line Mach-Zehnder interferometer (MZI) is fabricated by normal SMF-28 using a conventional fusion splicer (model IFS-9, INNO INSTRUMENT, Inc.) and a fiber-taper machine. As shown in Fig. 1, the sensor consists of three parts, i.e. two core-offsets and a fiber-taper. The two normal cleaved ends are made into one core-offset by one discharge. The other core-offset is also completed in the same way with a distance of 22.5 mm from the first one. To minimize the loss and achieve robust splices, the arc duration is set to 60% (1200 ms) and the current is 50% of the default value^[22]. A detection system consisting of a tunable laser (Agilent 81980A) and an optical power meter (Agilent 8163B) is used to measure the transmission spectra by wavelength sweeping. The wavelength range of tunable laser scans is 1465–1575 nm, and the rate is 5 pm per step. A transmission spectrum is obtained after the two core-offsets are fabricated (Fig. 2(a)). Then the sensor is placed in a fiber-taper machine to produce the abrupt taper between the two core-offsets. When the distance between the two core-offsets is stretched to 2000, 3000, 4000, and 4500 μm respectively, the transmission spectra are displayed in Figs. 2(b) and (c). When the sensor is stretched to 4500 μm , the maximum attenuation peak reaches 28 dB. The diameter of the taper waist is $D=91.70 \mu\text{m}$ and the last length of the sensor is 23 mm. The transmission spectra are revealed in Fig. 2(d) when the sensor is stretched to 4500 μm and cooled down to 25 $^\circ\text{C}$, in which the maximum attenuation peak moves to the left. The background loss of the interferometer is about 17 dB because when the fiber is fine-drawn at a high temperature, part of the lights in the cladding are scattered into the air.

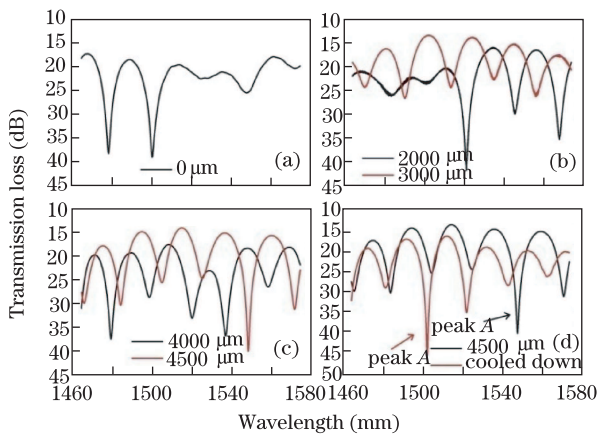


Fig. 2. (a) Transmission spectrum of the sensor with two core-offsets; the transmission spectra of the sensors when stretched to (b) 2000 and 3000, (c) 4000 and 4500, and (d) 4500 μm and cooled down to 25 $^\circ\text{C}$, respectively.

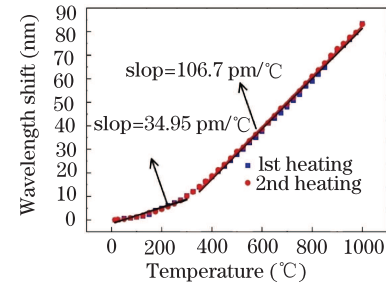


Fig. 3. Wavelength shifts with the increase of temperature, which are fitted separately for the twice heating processes.

According to Eq. (3), if the length of the sensor and effective RI change, the wavelength of the attenuation peak will shift with the external environmental condition. For the temperature testing, a muffle furnace with a heating range of 14–1000 $^\circ\text{C}$ is employed to heat the fiber interferometer. The interferometer is encapsulated in the furnace and heated at a fixed temperature rise rate of 5 $^\circ\text{C}/\text{min}$. Along with the temperature rising, the transmission spectra are recorded every other 25 $^\circ\text{C}$. The attenuation wavelength (peak A) shift as a function of the temperature is displayed in the process of twice heating in Fig. 3. According to Fig. 3, the sensitivities of the twice heating processes are almost the same, which reveals a high repeatability of the sensor. The curve can be divided into two linear sections. The slopes of the wavelength shifts with temperature in the range of 14–250 and 250–1000 $^\circ\text{C}$ are 34.95 ± 0.04 and $106.7 \pm 0.04 \text{ pm}/^\circ\text{C}$, respectively, by linear fitting.

The temperature sensitivity can be expressed by^[23]

$$d\lambda_m/dT = \left[\frac{\lambda_m}{\Delta n_{\text{eff}}} \left(\frac{dn_{\text{co}}}{dT} - \frac{dn_{\text{cl}}}{dT} \right) + \frac{\lambda_m}{L} \frac{dL}{dT} \right] / \left(1 - \frac{\lambda_m}{\Delta n_{\text{eff}}} \frac{\partial \Delta n_{\text{eff}}}{\partial \lambda} \right). \quad (4)$$

The change of the effective RI and the length of fiber with temperature are ignored under normal conditions. Hence the temperature sensitivity can be expressed by

$$d\lambda_m/dT = \frac{\lambda_m}{\Delta n_{\text{eff}}} \left(\frac{dn_{\text{co}}}{dT} - \frac{dn_{\text{cl}}}{dT} \right), \quad (5)$$

where $\frac{dn_{\text{co}}}{dT}$ and $\frac{dn_{\text{cl}}}{dT}$ are the thermo-optical coefficients of the fiber core and cladding respectively. The chemical composition of the fiber cladding is silicon dioxide, while the composition of the fiber core is silicon dioxide doped with germanium. The temperature sensitivity will increase with the increase of temperature, because the growth rate of $\frac{dn_{\text{co}}}{dT}$ is faster than that of $\frac{dn_{\text{cl}}}{dT}$. Thus the temperature curve is fitted separately during the whole range in Fig. 3.

The proposed MZI is placed on a mobile translation stage with the precision of 1 μm . The range for the measurement is 0–80 μm with an increasing step of 10 μm . The experimental process is conducted at room temperature, and air humidity is set to 20%. If the length of the sensor and increment of stretch length are denoted by L_{wo} and ΔL , respectively, the strain expression ε can be expressed by

$$\varepsilon = \frac{\Delta L}{L_{\text{wo}}}. \quad (6)$$

The wavelength shifts of attenuation peak *A* and peak *B* with the increase of strain are displayed in Fig. 4. The sensitivities of peak *A* and peak *B* are obtained by linear fitting, which are $5.91 \pm 0.01 \times 10^{-5}$ and $6.55 \pm 0.01 \times 10^{-4}$ nm/ $\mu\epsilon$, respectively. The strain sensitivity of peak *A* decreases one order of magnitude compared with that of the other MZI sensors, which are 0.31^[24] and -0.72 pm/ $\mu\epsilon$ ^[25] respectively.

RI measurement is carried out at room temperature, and salt solutions with different concentrations (0, 2, 4, 6, 8, 10, 12, and 14 g per 100 ml water respectively) are used to test the RI response. The corresponding RIs are 1.3329, 1.3364, 1.3397, 1.3429, 1.3460, 1.3490, 1.3519, and 1.3546, respectively. The maximum attenuation peak at 1570 nm is denoted. In Fig. 5, the spectral response is revealed by immersing the sensor in air and salt solutions with different concentrations. The wavelength shift of the maximum attenuation peak with the surrounding RI is a linear relationship for the external RI in the range of 1.3329 to 1.3546. The slope is only -12.14 ± 0.07 nm/RIU, which is low enough to decrease the cross sensitivity of RI for temperature sensing. The reported RI sensitivities of other MZI sensors that measured temperature and RI simultaneously are 66.32^[22] and 105.65 nm/RIU^[26], respectively.

In conclusion, a new MZI is proposed and fabricated by two core-offset attenuators and one abrupt taper in a SMF. When the proposed MZI is stretched to 4500 μm between two core-offset attenuators, an excellent MZI sensor is obtained, which has a prominent attenuation peak (~ 28 dB) and high temperature sensitivity. The fabricated MZIs are applied to measure temperature, strain, and RI changes. The temperature sensitivity is 34.95 ± 0.04 and 106.70 ± 0.04 pm/ $^{\circ}\text{C}$ in the temperature ranges of 14–250 and 250–1000 $^{\circ}\text{C}$, respectively. For temperature sensing, the proposed MZI is of low cross-

sensitivity with strain and RI. The fabrication process of the sensor is much simpler and has promising applications in high temperature sensing fields.

This work was supported by the National “973” Program of China (No. 2011CB013000) and the National Natural Science Foundation of China (Nos. 90923039 and 51105038).

References

1. P. Lu, L. Men, K. Sooley, and Q. Chen, *Appl. Phys. Lett.* **94**, 131110 (2009).
2. A. D. Kersey, *Opt. Fiber Technol.* **2**, 291 (1996).
3. T. Han, Y. Liu, Z. Wang, Z. Wu, S. Wang, and S. Li, *Opt. Express* **20**, 13320 (2012).
4. H. J. Patrick, A. D. Kersey, and F. Bucholtz, *J. Lightw. Technol.* **16**, 1606 (1998).
5. K. S. Chiang, Y. Liu, M. N. Ng, and X. Dong, *Electron. Lett.* **36**, 966 (2000).
6. J. F. Ding, A. P. Zhang, L. Y. Shao, J. H. Yan, and S. He, *IEEE Photon. Technol. Lett.* **17**, 1247 (2005).
7. F. Xu, C. Li, D. Ren, L. Lu, W. Lv, F. Feng, and B. Yu, *Chin. Opt. Lett.* **10**, 070603 (2012).
8. P. L. Swart, *Meas. Sci. Technol.* **15**, 1576 (2004).
9. Y. Yu, L. Jiang, B. Li, S. Wang, and H. Wu, *Chin. Opt. Lett.* **10**, 122801 (2012).
10. H. Y. Choi, M. J. Kim, and B. H. Lee, *Opt. Express* **15**, 5711 (2007).
11. Z. Tian and S. S. H. Yam, *IEEE Photon. Technol. Lett.* **21**, 161 (2009).
12. K. Kieu and M. Mansuripur, *IEEE Photon. Technol. Lett.* **18**, 2239 (2006).
13. O. Frazão, P. Caldas, F. M. Araújo, L. A. Ferreira, and J. L. Santos, *Opt. Lett.* **32**, 1974 (2007).
14. Z. Tian and S. S. H. Yam, *J. Lightw. Technol.* **27**, 2296 (2009).
15. T. Wei, Y. Han, H.-L. Tsai, and H. Xiao, *Opt. Lett.* **33**, 536 (2008).
16. Z. Ran, Y. Rao, J. Zhang, Z. Liu, and B. Xu, *J. Lightw. Technol.* **27**, 5426 (2009).
17. A. P. Zhang, L.-Y. Shao, J.-F. Ding, and S. He, *IEEE Photon. Technol. Lett.* **17**, 2397 (2005).
18. X. Chen, K. Zhou, L. Zhang, and I. Bennion, *Appl. Opt.* **44**, 178 (2005).
19. A. Iadicicco, S. Campopiano, A. Cutolo, M. Giordano, and A. Cusano, *Sens. Actuators B* **120**, 231 (2006).
20. L. Jiang, J. Yang, S. Wang, and M. Wang, *Opt. Lett.* **36**, 3753 (2011).
21. Z. Tian, S. S. H. Yam, and H. P. Loock, *Opt. Lett.* **33**, 1105 (2008).
22. B. Li, L. Jiang, S. Wang, L. Zhou, H. Xiao, and H. L. Tsai, *Sensors* **11**, 5729 (2011).
23. L. Xu, L. Jiang, S. Wang, B. Li, and Y. Lu, *Appl. Opt.* **52**, 2038 (2013).
24. A. Zhou, Q. Xu, T. Zheng, J. Yang, Y. Yang, and L. Yuan, *IEEE Photon. Technol. Lett.* **26**, 264 (2014).
25. Z. Cao, Z. Zhang, X. Ji, T. Shui, R. Wang, C. Yin, S. Zhen, L. Lu, and B. Yu, *Opt. Fiber Technol.* **20**, 24 (2014).
26. H. Sun, S. Yang, J. Zhang, Q. Rong, L. Liang, Q. Xu, G. Xiang, D. Feng, Y. Du, Z. Feng, X. Qiao, and M. Hu, *Opt. Fiber Technol.* **18**, 425 (2012).

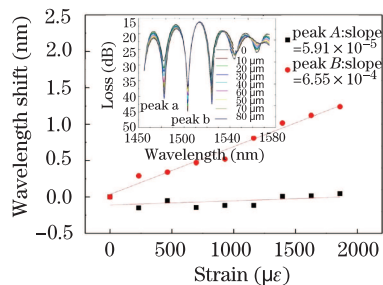


Fig. 4. Wavelength shifts of peak *A* and peak *B* with the increase of strain.

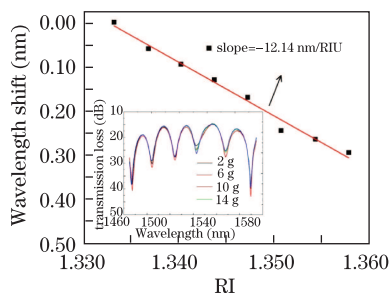


Fig. 5. Wavelength shifts of the maximum attenuation peak with the change of external RI.